

Article

Study of Atmospheric Plasma-Based Mass Separation System for High-Level Radioactive Waste Treatment

Sharif Abu Darda  and Hossam A. Gabbar *

Department of Energy and Nuclear Engineering, Faculty of Engineering and Applied Science, Ontario Tech University, Oshawa, ON L1G 0C5, Canada; sharifabu.darda@ontariotechu.net

* Correspondence: hossam.gabbar@ontariotechu.ca

Abstract: Solid spent nuclear fuel from nuclear power plants contains 3.4% fission products (80–160 amu), contributing to a radioactivity level of over 99.8%. On the other hand, liquid high-level radioactive waste (HLRW) from spent fuel reprocessing is composed of 98.9% bulk elements (0–60 amu) with 0.1% radioactivity. A separation mechanism for the mass categories into groups presents unique opportunities for managing HLRW in the long term with a considerable cost reduction. This paper proposes a thermal plasma-based separation system incorporating atmospheric-pressure plasma torches for HLRW mass separation into low-resolution mass groups. Several engineering issues must be addressed, such as waste preparation, waste injection into the plasma, and waste collecting after mass separation. Using the COMSOL Multiphysics simulation, the generic system can be studied using noble gas mass separation, and the mass filter capabilities can be further analyzed. This paper provides the history of plasma-based mass separation. The functional modelling of a thermal plasma mass separation system is proposed under atmospheric pressure. Finally, aspects of mass separation simulation using the noble gases argon and helium inside the plasma mass separation system are studied via COMSOL Multiphysics.

Keywords: thermal plasma; plasma-based mass separation; nuclear waste treatment; nuclear waste life cycle assessment; high-level radioactive waste treatment



Citation: Abu Darda, S.; Gabbar, H.A. Study of Atmospheric Plasma-Based Mass Separation System for High-Level Radioactive Waste Treatment. *Plasma* **2023**, *6*, 592–610. <https://doi.org/10.3390/plasma6030041>

Academic Editor: Andrey Starikovskiy

Received: 24 July 2023

Revised: 4 September 2023

Accepted: 6 September 2023

Published: 15 September 2023



Copyright: © 2023 by the authors. Licensee MDPI, Basel, Switzerland. This article is an open access article distributed under the terms and conditions of the Creative Commons Attribution (CC BY) license (<https://creativecommons.org/licenses/by/4.0/>).

Highlights

What are the main findings?

- High-level radioactive waste management.
- Plasma-based mass separation process design.

What is the implication of the main finding?

- Functional modelling of a mass separation system.
- Multiphysics simulation of plasma for a generic mass separation system in COMSOL.

1. Introduction

High-level radioactive waste (HLRW) is possibly the most toxic substance in the world. Because of high levels of induced radioactivity, HLRW must be stored for a long period of time and disposed of in complete isolation from humans and the environment. The primary source of HLRW is the spent fuel rods from nuclear reactors. The uranium fuel assemblies in a nuclear reactor are no longer efficient in fission. On average, a 1000 MWe pressurized water reactor (PWR) nuclear power plant holds 100 metric tons of reactor fuel assemblies [1]. One-third of the assemblies are spent and replaced with new ones, producing 25–33 tons of unprocessed spent nuclear fuel annually [2]. Fission products are the primary contributors to heat and penetrating radiation in spent fuel. The long half-life of some of the spent fuel radionuclides means that the spent fuel rods must be completely isolated, stored, and managed for a long time. This has led to the implementation of deep geological repositories

at about 200–1000 m for underground mines and caverns and 2000–5000 m for boreholes to store/dispose of HLRW as part of the long-term management of HLRW [3].

As of 2021, no commercial deep geological plants for HLRW storage/disposal are in operation. Until 2013, about 370,000 tons of heavy metal (tHMs) of spent fuel were discharged from the power reactors since the start of operation in the 1950s. About 120,000 tHMs were reprocessed for reuse and plutonium extraction. The inventory of HLRW worldwide increases by about 12,000 tHMs every year. All HLRW worldwide is stored in a temporary storage facility until more permanent solutions arrive [4]. After being removed from the reactor, the spent fuel is stored in the spent fuel pool for 3–5 years, and for a maximum of 20 years [5]. Then, the fuel assemblies are transferred to dry cask storage for 100 years [6]. It costs about USD 1 million for each cask to build and another USD 500,000 to load each one with 10–12 tons of spent fuel [7,8] because of the cask's increased radiation protection and special material assembly requirements. Moreover, a long-term maintenance cost is also associated with the security of the casks.

According to the mass profile, spent fuel rods are composed of approximately 3–4% fission products, the most radioactive elements, which contribute to 99.8% of the radioactivity via gamma and beta emissions; the remaining 96–97% masses are actinides that contribute to long-term and 0.2% overall radioactivity, primarily through alpha emissions [9]. In the case of liquid HLRW from spent fuel processing, like the Hanford site, 98.9% of the mass consists of non-radioactive bulk elements with 0.1% radioactivity, 0.7% fission products with 99.7% radioactivity, and 0.4% actinides with 0.2% radioactivity. Separating fission products from the bulk elements and actinides in solid, spent fuel and liquid forms of HLRW provides a unique HLRW management solution for the long term. Fission products generally have a mass of 80–160 amu, whereas actinides have a mass of 225–250 amu, and elements whose mass is <65 amu can be considered non-radioactive bulk elements. A traditional spent fuel processing plant can separate the actinides from the fission products. The process also creates a large residue volume of liquid HLRW as the first and second cycles of raffinate liquid mainly contain nitric acid, fission products, and minor actinides besides uranium and plutonium [9,10]. A thermal plasma-based mass separation system provides a unique opportunity for separating the bulk elements, fission products, and actinides as a mass group with high throughput without producing residual waste. The separated transuranic elements like uranium and plutonium can still be used as reactor fuel in the form of MOX (metal oxide) fuel for current and generation IV reactors [11]. Due to the high radioactivity of fission products (3–4%), current practice involves storing 100% of spent fuel mass for a long time. A 96% volume reduction is possible with a state-of-the-art plasma mass separation to separate the fission products and store them in dry cask storage until a more permanent solution is available. This way, the storage volume of HLRW can be reduced dramatically. Even if the actinides are not reused as reactor fuel, they present less radiation risk than the fission products and will require fewer safety measures while in storage.

The world's fossil fuel supply is running low and is estimated to end in a century. Subsequently, renewable sources are still relatively costly for energy production. Humanity needs to build more nuclear power plants to support future energy demands, which will increase the HLRW inventory rapidly. An effective HLRW disposal for the future requires separation techniques for fission products with high throughput. This paper provides a background on rotating plasma-based mass separation technologies for HLRW. Later, functional modelling of a thermal plasma mass separation system is proposed using inductively coupled plasma under atmospheric pressure. The mass separation system operation is based on the band gap ion mass filter principle proposed by Ohkawa et al. [12]. Furthermore, a study of multiphysics simulations using noble gases (argon, helium), plasma, and a temperature profile on the mass separation system under cross-electric and magnetic fields was carried out.

2. Plasma-Based Mass Separation

2.1. Mass Separation Experiments

Plasma mass separation provides a unique opportunity for radioactive waste long-term management, especially for HLRW. Using plasma for element separation based on mass is not new. The first time plasma mass separation was used was in Calutrons in the Manhattan Project during WWII [13,14], where the U-235 atoms were separated from U-238 to make a concentrated uranium bomb. The first rotating thermal plasma experiment for ion mass separation was conducted in Sweden from 1966 to 1971 using H, D, He, and Ar gases [15]. Another plasma mass separation experiment was conducted at Yale University from 1980 to 1997 as a plasma centrifuge [16], which was later refined as a vacuum arc centrifuge in Australia [17] and Brazil [18]. The original plasma centrifuge had a metal cathode in which materials were subject to separation. A 4 kV voltage was applied to the cathode to produce a vapor plasma in a magnetic field of 7 kG (0.7 T). The materials used for the cathode were various metal isotopes or elements such as Cu/Zn and their isotopes, C, Al, Mg, Zn, Cd, Pb, etc. [19]. Although no practical device was built to demonstrate the plasma centrifuge in HLRW mass separation, the concept was presented as one of the potential mass separation methods for HLRW management through mass separation by Abraham J. Fetermana and Nathaniel J. Fischa from the Department of Astrophysical Sciences, Princeton University, in 2011 [9].

One of the most prominent plasma mass separation experiments was carried out by a private company named Archimedes Technology in San Diego from 1998 to 2005 on the single-particle ion orbit theory (band gap theory) T. Ohkawa [12]. A demo system was built to generate a helicon plasma in a chamber of 3.9 m in length and 0.4 m in diameter with a magnetic field of 1.5 kG. For separation, only a DC voltage component was used. The plasma was heated with ~3 MW, 6 MHz RF power and driven with end electrodes biased at ≤ 700 V [20]. Although no actual HLRW mass separation was performed using the demo device, a few initial noble gas mass separation and Na and Bi [21] mass separation experiments showed promising results. The demo device addressed significant mass separation physics and the processes for rotating plasma and high throughput, but no actual separation of HLRW was published [22].

Since 2010, the most active experiments on plasma-based mass separation have been carried out at Irkutsk, Russia [23], plasma mass filter experiments (PMFX) at Princeton Plasma Lab [24], and spent nuclear fuel (SNF) processing at the Joint Institute for High Temperatures in Moscow [25]. Table 1 lists all the previous experiments of plasma-based mass separation until now.

Table 1. Plasma mass separation experiments over the years [19]. Copyright 2018 AIP Publishing LLC.

Devices (Location)	Working Species	Year(s)
Calutron (Berkeley, ORNL)	U isotopes	1941–1998
FI torus (Sweden)	H/Ar	1966–1971
ICRH (US, Russia, France)	Many isotopes/elements	1976–present
Plasma centrifuge (Yale)	Metal isotopes and elements	1980–1987
Vacuum arc centrifuge (Australia)	Cu/Zn and their isotopes	1989–1999
Vacuum arc centrifuge (Brazil)	C, Al, Mg, Zn, Cd, Pb, etc.	1987–1998
Archimedes filter (San Diego)	Xe/Ar and Cu/Ag/Au?	1998–2005
Linear device with electrodes (Kyushu)	Ar and Xe	2007
POMS-E-3 (Irkutsk)	N, Ar, and Kr	2010–present
Vacuum arc separator (Irkutsk)	Ni, Cr, Fe, and W	2011–2015
PMFX (PPPL) Ar/Kr 2013–2014	Ar/Kr	2013–2014
SNF separator (JIHT Moscow)	U, Gd, and He	2013–present

2.2. Plasma-Based Mass Separation for High-Level Nuclear Waste Remediation

Of all the plasma-based mass separation experiments, plasma centrifuge, Archimedes filter, plasma mass filter and SNF separator system are applicable for nuclear waste mass separation, especially HLRW and spent nuclear fuel [9,12,19,25]. The Archimedes filter, plasma mass filter, and SNF separator system are applicable for separating elements (atoms) in a mass group rather than individual elements. In traditional chemical separation like UREX (URanium EXtration), PUREX (Plutonium and Uranium Recovery by EXtraction), and TRUEX (TRansUranium Extraction), the separation works on separating certain atoms at a time in a chemical mixture [26]. The process is a time-consuming and multi-stage process. In the case of plasma mass separation for HLRW, the separation will focus on separating the fission products as a group with a mass profile of 80–160 amu rather than, for example, separating Cs-137 (standard fission products). The throughput of plasma mass separation will be determined as the rate at which waste can be processed in a mass separation system, and the separation factor will depend on a group of species i , in the output and input waste, which can be defined as

$$\text{Separation factor } \alpha = \frac{\text{Fraction of group } i \text{ in output products}}{\text{Fraction of group } i \text{ in the input products}} \quad (1)$$

The plasma mass separation aims to separate the fission products from spent fuel (group i). Additionally, plasma mass separation provides a greater chance of separating fission products in HLRW in a single stage than traditional chemical-based separation. The HLRW mass separation goal is to achieve a cutoff mass between the high and the low mass group. Table 2 lists the separation goal for various HLRW with a mass cutoff in amu.

Table 2. HLRW's plasma mass separation goal.

Application	Cutoff Mass (amu)
Spent fuel rod	~200
HLW from reprocessing	~80

Until 2013, about 120,000 tHM of spent fuel from nuclear reactors was reprocessed worldwide, primarily by the USA, France, India, Japan, Russia, and the United Kingdom. PUREX is the most common chemical separation process for spent fuel reprocessing, where uranium and plutonium are extracted from the spent nuclear fuel in a chemical process. There are several issues with the PUREX process. Firstly, the PUREX process is not economical with respect to the direct storage/disposition of waste and using fresh uranium fuel, as the process is a multi-stage continuous solvent extraction process. Currently, most nuclear countries use a once-through fuel cycle where the spent fuel is not reprocessed but stored directly as HLW in dry casks. This is due to the relatively low cost of new uranium fuel compared to reprocessing. The second issue with PUREX is that it produces a separate stream of uranium and plutonium, which has a greater risk of nuclear proliferation. The third issue with PUREX is that it creates more residual waste. Although about 96% of the original spent fuel mass can be extracted (95% uranium and 1% plutonium), this leaves a large amount of nitric acid solution containing the remaining intensely radioactive 3–4% fission products of the original spent fuel mass, making the whole solution HLW, with some ILW and LLW containing transuranic elements separated during the process. Plasma mass separation can address the nuclear proliferation issue as the waste will be separated as a mass group of all the transuranic elements instead of individual actinides.

Additionally, replacing multi-stage chemical separation with single-stage plasma separation will reduce residual waste production in chemical separation. It is estimated that after using PUREX to extract uranium and plutonium from the spent nuclear fuel, the remaining 95% of the mass is nitric acid introduced by the reprocessing [27]. This liquid solution is stored as high-level liquid radioactive waste (HLLRW). This liquid waste must

be vitrified for long-term storage/disposal for proper immobilization. Since plasma mass separation will operate on high-temperature plasma, no liquid waste will be generated. Additionally, the actual waste output can be collected as vitrified waste that will ensure the immobilization of the waste and dramatically reduce the waste storage/disposal volume in the long term.

In terms of cost, Table 3 lists the life cycle cost of HLRW management with the currently available technologies.

Table 3. Life cycle cost analysis (LCCA) of high-level waste management (in 2003 USD value validated in 2017) [28–34].

Method		Unit	USD	Cost Breakdown
Reprocessing	THORP and UP-3	USD/kgHM	1760	~6 B USD capital cost, 10 years of operation with 800 tHM/y processing capability, refurbishment and decommissioning 30% capital cost
	Government-owned	USD/kgHM	1350	30 years operation period
	Privately owned	USD/kgHM	2000	30 years operation period and guaranteed rate of return
Dry cask interim storage	On-site	USD/kgHM	110–130	1000 tonnes facility, 40 years lifetime. 10 M USD capital cost
	Off-site	USD/kgHM	210–275	
MOX fuel fabrication		USD/kgHM	1500	Recovered plutonium oxide mixing with uranium oxide
Deep Geological Repository *	CANDU	USD/KgHM	100	3.6 M USD fuel bundle, 2.5 B USD capital and 7 B USD, in 30 years of operation and closure
	LWR	USD/KgHM	400	30 years of operation and closure

* after 30 years of interim storage.

For plasma mass separation to dramatically change HLRW processing in the future, the process should cost USD200/kgHM [31] since the plasma mass separation system has a relatively smaller footprint than other systems, in addition to reduced construction, maintenance, and operation costs. Additionally, with zero additional cost of vitrification for waste immobilization, a 2 B USD budget for processing 500 tHM in 20 years would keep the processing cost < USD200/kgHM [9].

3. Functional Modelling of a Generic Plasma-Based Mass HLRW Separation System

Most of the current plasma-based mass separation technologies have some practical limitations because they operate in a high vacuum, meaning a minimum energy investment is necessary for ionizing and heating the atoms, and they have a low density relative to atmospheric pressure plasma that restricts their throughput [19]. They are nearly collisionless ion gyro-orbits or ion drifts in electric and magnetic fields. However, highly collisional plasmas are also interesting for mass separation since they occur at relatively high densities, which could produce high throughput, and at relatively low temperatures, reducing the need for auxiliary plasma heating. This is where the atmospheric-pressure plasma torch can be advantageous in high-density, highly collisional, and continuous operation with respect to low-density, near-collisionless, and batch operation. Plasma mass separation is a complex thermochemical process with various stages involved. As previously discussed, Archimedes' demo filter, based on the band gap ion mass filter principle by T. Ohkawa and colleagues, separates ions in a plasma based on the m/z ratio. It utilizes cross-electric and magnetic fields in cylindrical geometry where only a DC radial parabolic voltage is applied [12]. This paper investigates the principle of mass separation in atmospheric pressure plasma. A convenient way to identify the stages/processes involved will be to design a functional model representing the process with its variables. A functional model represents the functions (activities, actions, processes, operations) within the modelled system or subject area in system engineering. Functions translate needs into a physical

structure that will meet those needs. Function modelling is the formal way to define and model functions [35]. In plasma-based mass separation for HLRW, the process has five main tasks or stages: waste preparation, waste injection, waste ionization, waste mass separation, and finally, waste collection. There are multiple activities in each stage. Various physical processes are involved in each stage of the process. The functional model of a proposed generic plasma mass separation is shown in Figure 1.

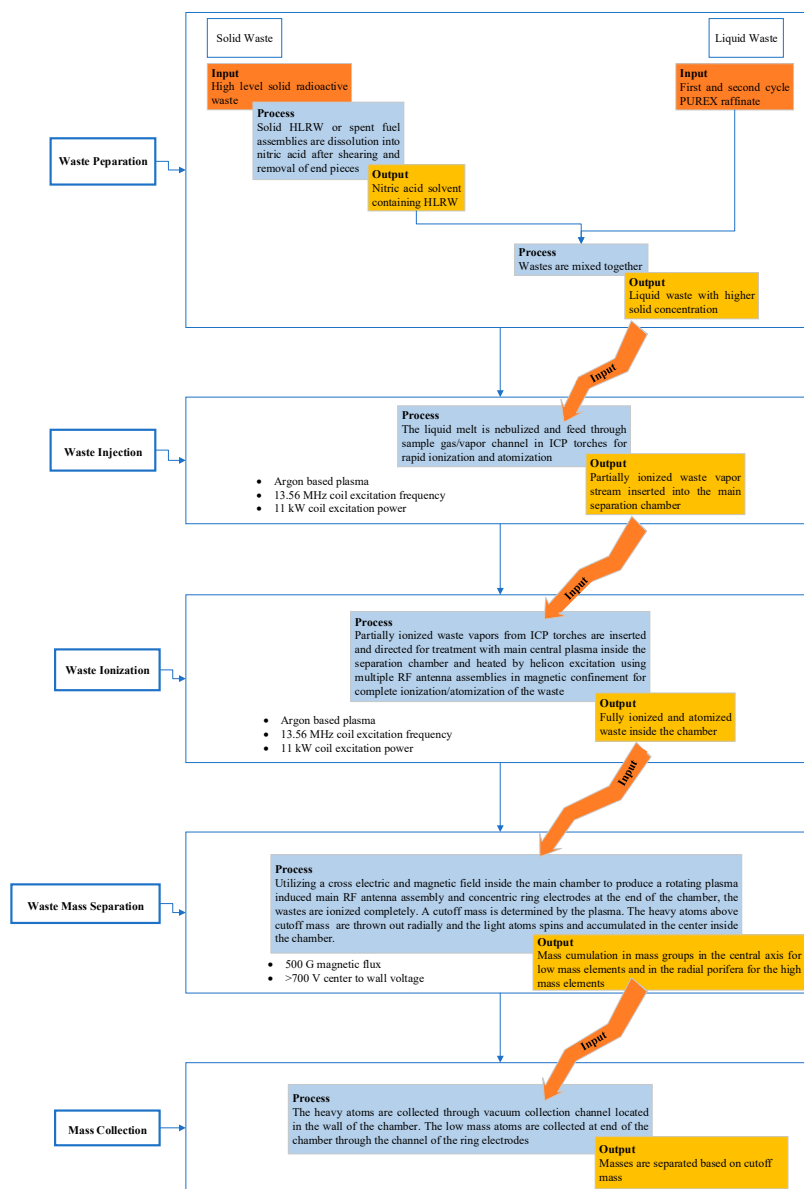


Figure 1. Functional model of proposed plasma-based mass separation for HLRW.

A rotating plasma utilizes a cross-electric and magnetic field to separate ions inside the plasma chamber based on a cutoff mass. Based on the functional model, a generic mass separation system incorporating two atmospheric-pressure inductively coupled plasma (ICP) torches connected in series was proposed. A cross-electric and magnetic field is applied in the second ICP chamber. A 2D-asymmetric generic mass separation system was designed in COMSOL for initial noble gas ICP simulation under mass separation conditions. A cross-sectional view of the proposed generic mass separation system highlighting its components is shown in Figure 2, and a 3D model of the system is shown in Figure 3. The parts marked in numbers are listed in Table 4.

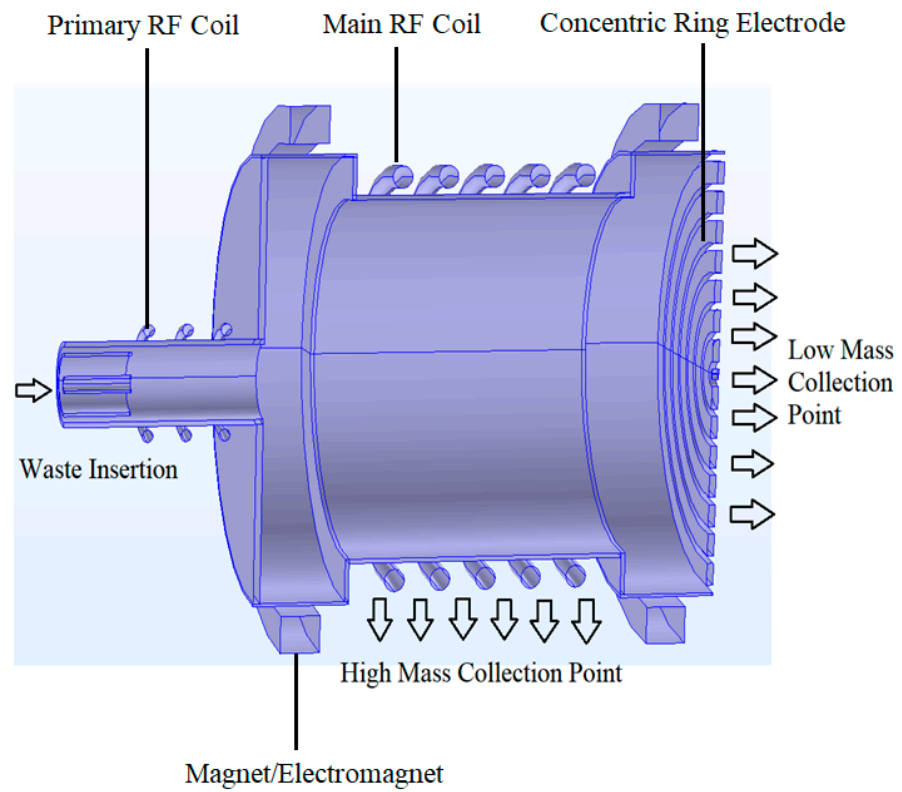


Figure 2. Cross-section of proposed generic plasma-based mass separation system for HLRW.

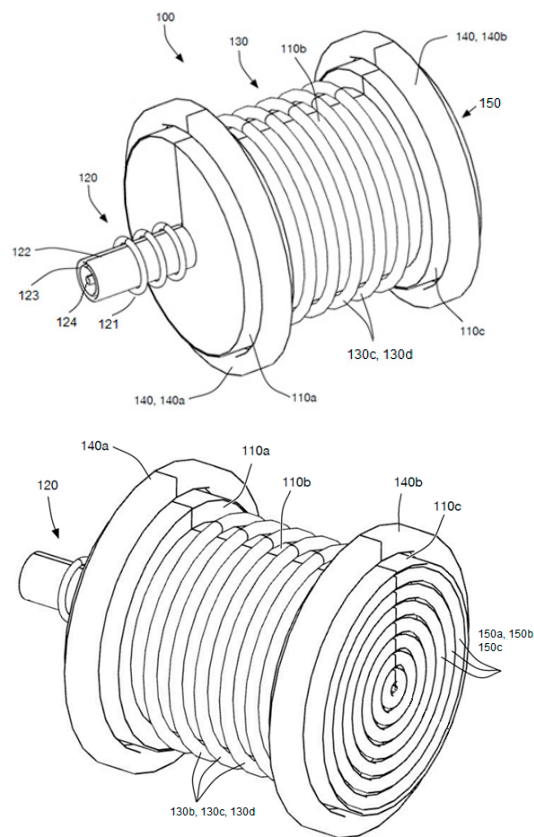


Figure 3. Generic plasma-based mass separation system for HLRW.

Table 4. List of parts in the mass separation system.

Components		Details
100		Mass separation system
110 (110a, 110b, 110c)		Separation apparatus
120 (121, 122, 123, 124)	Primary RF ICP torch (RF coils, sheath wall, central wall, carrier wall)	
130 (130b, 130c, 130d)		Main RF ICP torch (RF coils)
140 (140a, 140b)		Electromagnets (coils)
150 (150a, 150b, 150c)		End electrodes (concentric rings)

3.1. Waste Preparation

Waste preparation is the primary stage of the whole process. This stage determines the suitable waste form to inject into the mass separation system for proper ionization in the system plasma. There are two main forms of HLRW: solid waste (spent fuel (SP) assemblies) and liquid waste from spent fuel reprocessing. For mass separation of HLRW, the suitable waste form for RF plasma torch injection is liquid waste through a carrier gas channel. Therefore, the spent fuel assemblies' solid waste needs to be liquified after shearing and end piece removal. The process is well known and practiced worldwide in PUREX and UREX processes. The spent fuel is liquified by dissolving spent fuel into HNO_3 to make $\text{UO}_2(\text{NO}_3)_2$ (aq), $\text{Pu}(\text{NO}_3)_4$ (aq) and nitrates of other metals. This aqueous solution is perfect for waste injection into the mass separation chamber. Later, this liquid solution can be mixed with the first- and second-cycle PUREX raffinate (liquid HLRW) to raise the total solid concentration.

3.2. Waste Injection

The liquid waste from the waste preparation phase can then be nebulized through the central carrier channel (parts 124 in Figure 3) of the primary RF ICP torch shown in Figure 2 for ionization in the plasma flame. The plasma torch is an RF ICP torch with argon as the plasma gas supplied through the central and sheath channels (parts 122 and 123 in Figure 3). Nebulizing waste into fine droplets for injection instead of liquid injection ensures rapid, homogenous distribution of waste into plasma with less chance of plasma fluctuation. The waste vaporized via nebulization can then be rapidly heated by the torch's >7000 K plasma temperature in the coil region. This temperature was achieved at the center of the plasma flame using an RF power supply generating an 11 kW coil excitation power supplied through the primary RF coils (parts 121x) and with a 13.56 MHz excitation frequency [36] by COMSOL RF ICP simulation and an initial experiment with RF ICP plasma using pure argon gas. Waste injection through the carrier channel will expose the waste to a higher temperature at the center of the plasma for fast ionization. The waste is expected to be partially ionized and produce high-temperature waste vapor before exposure to the separation chamber's central RF plasma. The advantage of using an atmospheric pressure ICP for both the injection and the mass separation of waste is that the waste injection can be continuous, whereas other high vacuum systems are usually capable of batch treatments [37].

3.3. Waste Ionization

Partially ionized waste vapor from the primary plasma torch will be directed into the main separation chamber. The waste will be fully ionized and atomized by the central filter plasma generated with a five-turns RF coil assembly (parts 130 in Figure 3) bounded by magnets/electromagnets on the opposite end. The central plasma in the separation chamber utilizes the primary RF ICP plasma outlet as an inlet or plasma gas. The multiphysics simulation using COMSOL shows that using an 11 kW coil excitation power for both primary and central RF coils with a 13.56 MHz coil frequency, the temperature achieved inside the separation chamber is >9000 K. In mass spectrometry, using an atmospheric

pressure ICP ionization method compared to other ionization methods is considered a hard ionization method to ensure complete sample atomization during sample ionization [38]. Since the mass separation of waste is solely dependent on the ionization $Z = +1$ of waste elements for separation in a mass group, two stages of waste ionization will ensure the waste materials are fully ionized with high temperatures generated by the primary RF plasma torch and later by the central plasma before mass separation. This double plasma treatment of waste will ensure maximum ionization of the waste for mass separation.

3.4. Waste Mass Separation

The band gap ion mass filter principle says that ions can be radially separated based on the mass range with a combination of an axial magnetic field and radial or azimuthal electric field in cylindrical confinement [12]. A cross-electric and magnetic field influences the fully ionized waste for ion mass separation inside the main cylindrical separation chamber. The magnetic field is generated using two circular electromagnets or permanent magnet rings at each end of the central RF coil (parts 140 in Figure 3). An electric field proportional to r can be imposed using a set of concentric ring electrodes at the axial ends of the cylinder. Although the band gap mass filter principle is operated under a high vacuum with low, dense, collisionless plasma, our study with atmospheric plasma simulation (Section 4) shows the operation can be transparent to atmospheric plasma where the plasma is highly dense and heavily collisional. When the electrode's voltage has AC and DC components, the ion orbit characteristics show a bandgap structure like electrons in a semiconductor with few confined and unconfined spaces [12,39]. The bandgaps can be graphically represented in the α - β space on the x and y axes, respectively, where α represents the ratio of the potential difference across the filter to the total kinetic energy of the ion while the parameter β represents the ratio of the band gap's width to the ion's total kinetic energy. The parabolic band curve separates the regions as confined and unconfined regions for the range of α and β values for which ions with a particular mass-to-charge ratio are radially confined in the filter, while the masses above the certain mass-to-charge ratio are not confined radially [12]. For a case of $\beta = 0$ and the electrode's voltage with only DC voltage components while $V_{rf} = 0$, the ions with mass/charge $> m_{cutoff}$ are radially unconfined

$$\frac{m_c}{Z} > \frac{eB^2a^2}{8V_{dc}} \equiv m_{cutoff} \quad (2)$$

where A_{Cutoff} = cutoff atomic weight/mass, m_c = mass of the cutoff atom, z = ion charge, B = magnetic field, R_{Wall} = plasma radius, V_{dc} = center to wall voltage, and e = electron charge. For the hydrogen ion mass, considering the base mass $m_c = m_H$ and $V_{dc} = V_0$, Equation (2) can be rewritten as

$$A_{cutoff} = \frac{ZeR^2B^2}{8V_0m_H} \quad (3)$$

Under mass separation conditions, ions above the cutoff mass are not confined and thrown to the radial wall. In contrast, the ions below the cutoff mass are contained in the center of the chamber's axial direction.

3.5. Mass Collection

After the mass separation of waste, the separated high-mass ions above the cutoff mass and the low-mass ions below the cutoff mass are collected in the different waste collectors. Since the high-mass ions are thrown into the radial wall, a negative pressure suction channel on the radial wall can take the high-mass ions out of the chamber. The low-mass ions that accumulate in the center of the plasma and the chamber can be collected through the light mass collection point opposite the waste injection channel shown in Figure 2. One added advantage of the proposed mass separation unit shown in Figure 2 is that the separated low-mass ions will be pushed to the system's edge, where the waste will be collected due to the input pressure. It is essential to mention the waste insertion and

collection mechanism depending on the temperature. Rapid heating is necessary for waste insertion, whereas rapid cooling is essential for collecting waste output. Both heavy and light collector systems are considered separate units from the mass separation system so that they can be periodically disconnected and cleaned.

Additionally, any waste removal through suction would affect the plasma stability and temperature. This paper presents a study of mass separation at atmospheric pressure. Further research must be carried out on the effect of waste collection on the separation and system plasma stability.

4. Mass Separation Simulation of ICP for Noble Gas inside Mass Separation Unit

A simulation analysis was conducted using the COMSOL multiphysics tool using the generic mass separation unit proposed in Section 3 to investigate the mass separation effect under atmospheric pressure. Pure, noble gases, argon and helium, are used to analyze mass separation under atmospheric pressure in separate simulations under the same parameters. The model in Figure 2 was developed using COMSOL Multiphysics software, version 6.1, released in December 2022. In COMSOL, RF, ICP is modelled with an equilibrium discharge (ED) interface. The interfaces for ED are appropriate for modelling any thermal plasmas (i.e., arcs or inductively coupled discharges). Where partial to complete local thermodynamic equilibrium (LTE) conditions of the thermal plasma are assumed [40], these plasmas can be modelled using the magnetohydrodynamics (MHD) equations because these kinds of plasma can be considered conductive fluid mixtures at the macroscopic level. The motion of the conducting fluid in an electromagnetic field is described by MHD, which later combines the Navier–Stokes, heat, and Maxwell’s equations. The plasma’s chemical makeup is disregarded in this case. Modelling plasma in COMSOL multiphysics using the ED interface is based on a set of assumptions that lead to simplifications of the MHD equations:

1. The plasma is fully ionized (a mixture of electrons and ions).
2. The plasma optically thin is under local thermodynamic equilibrium (LTE) conditions.
3. The plasma is considered a locally neutral Newtonian fluid mixture.
4. The plasma flow is laminar and quasi-incompressible under atmospheric pressure.

4.1. Mathematical and Physical Model

Four physics interfaces are used in ED for the mass separation model simulation in COMSOL: Magnetic Fields (MF), Heat Transfer in Fluids (HTF), Electric Current (EC) and Laminar Flow (LF) interfaces. There are additional multiphysics couplings: Magnetohydrodynamic (M) (Magnetic Fields and Laminar Flow), Equilibrium Discharge Heat Source (EDHS) (1. Magnetic Fields and Heat Transfer in Fluids, 2. Electric Current and Heat Transfer in Fluids), Equilibrium Discharge Boundary Heat Source (EDBHS) (1. Electric Current and Heat Transfer in Fluids, for the anode, 2. Electric Current and Heat Transfer in Fluids, for cathode), Static Current Density Component (SCDC) (from Electric Current and Magnetic Field), Induction Current Density Component (ICDC) (from Magnetic Field to Electric Current), and finally, Nonisothermal Flow (NF) (Laminar Flow and Heat Transfer in Fluids). The ED can be described by a set of equations defined in the physics interfaces constituting the different multiphysics interfaces. Note that all the physics features in the individual physics interfaces are also available in the multiphysics interface. The MF interface solves Ampère–Maxwell’s equations formulated using the magnetic vector potential and, optionally for coils, the scalar electric potential as the dependent variables. The M couples Lorentz force and electromagnetic force. In addition to Ampere’s law, the following equations are solved under the MF interface and M multiphysics node in the frequency domain, assuming time-harmonic fields:

$$\nabla \cdot J = 0 \quad (4)$$

$$\nabla \cdot H = J \quad (5)$$

$$B = \nabla \cdot A \tag{6}$$

$$J = \sigma E + j\omega D + \sigma v \times B + J_e \tag{7}$$

$$E = -j\omega D \tag{8}$$

$$F = \frac{1}{2} \text{Re}(J \times B^*) \tag{9}$$

$$J = \sigma(E + v \times B) \tag{10}$$

where $\nabla, H, J, B, A, E, D, \sigma, v, J_e, j, \omega$ are the divergence, magnetic field intensity, current density, magnetic flux density, magnetic vector potential, electric field intensity, electric displacement or electric flux density, electrical conductivity, the velocity of the conductor, externally generated current density, imaginary unit, and angular frequency, respectively. In the HTF interface and EDHSs, multiphysics coupling features solve the energy conservation equation under frequency stationary study: in fluid,

$$\rho C_p \mathbf{u} \cdot \nabla T + \nabla \cdot \mathbf{q} = Q + Q_p + Q_{vd} \tag{11}$$

$$\mathbf{q} = -k \nabla T \tag{12}$$

$$\rho = \frac{p_A}{R_s T} \text{ in an ideal gas domain} \tag{13}$$

In solid,

$$\rho C_p \mathbf{u} \cdot \nabla T + \nabla \cdot \mathbf{q} = Q + Q_{ted} \tag{14}$$

where the source of heat Q (W/m^3) includes three source/sink components:

1. Resistive heating (ohmic heating):

$$Q = \mathbf{J} \cdot \mathbf{E} \tag{15}$$

2. Volumetric net radiation loss Q_{rad} is defined by the total volumetric emission coefficient, which is a material property.
3. Enthalpy transport (energy carried by the electric current):

$$\frac{\partial}{\partial t} \left(\frac{5k_B T}{2q} \right) (\nabla T \cdot \mathbf{J}) \tag{16}$$

where $\rho, C_p, \mathbf{u}, k_B, T, \mathbf{q}, Q_p, Q_{vd}, Q_{ted}, p_A,$ and $R_s,$ are density, specific heat at constant pressure, mass averaged fluid velocity vector, Boltzmann constant, temperature, thermal conductivity, pressure work, viscous dissipation, thermoelastic damping, absolute pressure, and specific gas constant, respectively. The EC interface and EDBHSs, SCDC, and ICDC multiphysics coupling features solve a current conservation equation based on Ohm's law using the scalar electric potential as the dependent variable. Ohmic heating and induction heating, when heat transfer is coupled together with electrical or electromagnetic interfaces:

$$\nabla \cdot \mathbf{J} = Q_{j,v} \tag{17}$$

$$\mathbf{J} = \sigma \mathbf{E} + \mathbf{J}_e \tag{18}$$

$$\mathbf{E} = -\nabla V \tag{19}$$

$$\mathbf{J}_{mf} = \mathbf{J}_{e,mf} \tag{20}$$

$$\mathbf{J}_{e,mf} = -\sigma \nabla V \tag{21}$$

$$\mathbf{J}_{ec} = -\sigma \nabla V + \mathbf{J}_{e,ec} \tag{22}$$

$$J_{e,ec} = 0 \tag{23}$$

For the anode,

$$-\mathbf{n} \cdot (-k\nabla T) = Q_b \tag{24}$$

$$Q_b = |\mathbf{J} \cdot \mathbf{n}| \Phi_s \tag{25}$$

For the cathode,

$$Q_b = -J_{ele} \Phi_s + J_{ion} V_{ion} \tag{26}$$

$$J_{elec} = if(|\mathbf{J} \cdot \mathbf{n}| > J_R, J_R, |\mathbf{J} \cdot \mathbf{n}|) \tag{27}$$

$$J_R = A_R T^2 \exp\left(-\frac{q\Phi_{eff}}{k_B T}\right) \tag{28}$$

$$J_{ion} = |\mathbf{J} \cdot \mathbf{n}| - J_{elec} \tag{29}$$

where $Q_{j,v}$, J_{mf} , $J_{e,mf}$, J_{ec} , $J_{e,ec}$, k , Φ_s , Q_b , J_{ele} , J_{ion} , V_{ion} , J_R , A_R , q , and Φ_{eff} , are the volumetric source of current, current density due to magnetic field, the external current density in the magnetic fields, current density due to electric current, the external current density in the electric currents, thermal conductivity, surface work function for anode and cathode, boundary heat source, electron current, ion current, the ionization potential of the plasma, Richardson–Dushman current density, Richardson’s constant, electronic charge, and the effective work function of the surface, respectively. Finally, the LF interface and NF multiphysics coupling solve continuity, momentum, and energy equations as follows under stationary and weakly compressible flow conditions:

Continuity:

$$\nabla \cdot (\rho \mathbf{u}) = 0 \tag{30}$$

Momentum:

$$\rho(\mathbf{u} \cdot \nabla)\mathbf{u} = \nabla \cdot [-p\mathbf{I} + \mathbf{K}] + \mathbf{F} \tag{31}$$

$$\mathbf{K} = \mu(\nabla\mathbf{u} + (\nabla\mathbf{u})^T) - \frac{2}{3}\mu(\nabla \cdot \mathbf{u})\mathbf{I} \tag{32}$$

$$Q_{vd} = \tau : \nabla\mathbf{u} \tag{33}$$

The Lorentz force acting on the fluid is defined in the magnetic field interface:

$$\mathbf{F} = \mathbf{J} \times \mathbf{B} \tag{34}$$

where p , τ , Q_{vd} , \mathbf{F} , μ , \mathbf{I} , and \mathbf{K} are the pressure, viscous stress tensor, viscous dissipation, volume force vector, dynamic viscosity, identity matrix, and dimensionless resistance coefficient, respectively.

4.2. Results and Discussion

A 2D-axisymmetric model of the mass separation unit was designed in COMSOL, shown in Figure 4, for separate argon and helium plasma-based generic mass separation simulation. Although a mass separation simulation using mixed argon and helium gas would be a more accurate and obvious choice, the current COMSOL multiphysics version 6.1 does not support a mixed gas ICP plasma modeling under the ED interface instead of a single plasma gas (i.e., air, argon, helium, nitrogen, etc.). Table 5 shows the parameters used to develop the mass separation unit and the ICP simulation for different noble gases. Quartz was used in the simulation as the material for the three-channel primary RF IPCT. Both the primary and central RF coil material were defined as copper. The electromagnetic field coil material was also defined as copper. In the case of the main separation chamber, the bottom wall and the radial wall section underneath the central RF coils are defined as quartz. At the same time, the top wall has concentric rings and the radial wall section underneath the electromagnetic field coil is defined as graphite for conductivity. The chamber was 0.35 m long and had a radius of 0.14 m in the coil region.

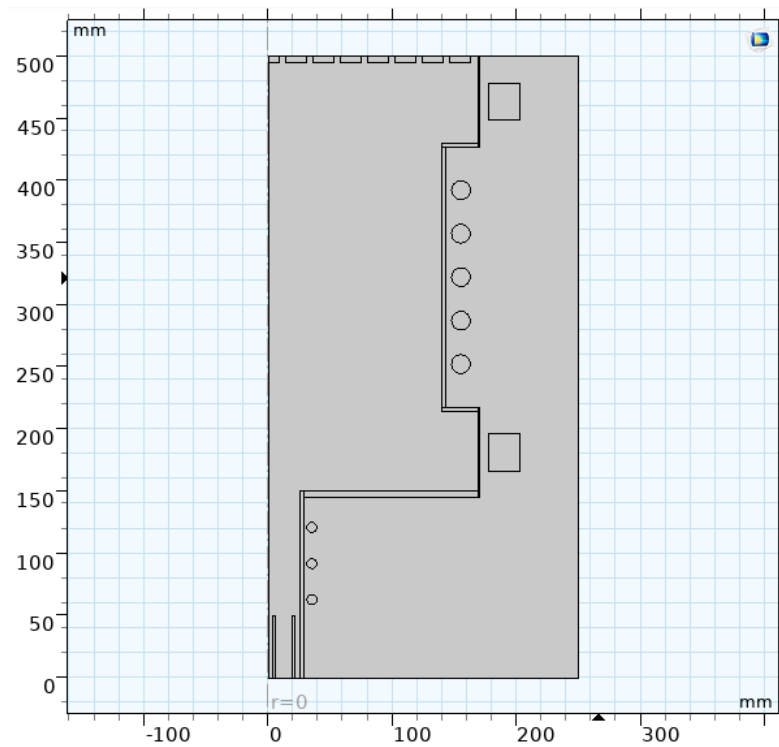


Figure 4. A 2D axisymmetric model of the mass separation unit in COMSOL.

Table 5. Plasma-based mass separation simulation parameters.

Parameter	Value
$L_{ }$ (axial length)	0.35 m
a (radial width)	0.14 m
Magnet	electromagnet
Gas velocity	0.1–0.13 m/s
$B_{ }$ (magnetic field)	0.02–0.037 T
P_{rf} (RF power)	11 kW
Z (ion charge)	1
Voltage	≤ 20 –25 V

Using the parameters from Table 5, simulation was carried out in multiple stages. First, only the primary RF ICP torch (ICPT) connected to the separation chamber was analyzed, using an RF power of 11 kW and an average gas velocity of 0.12 m/s through all three channels of the primary RF ICPT (laminar gas flow). The carrier, central, and sheath channels had thicknesses of 2 mm, 2.2 mm, and 3.5 mm, and inner radii of 3.7 mm, 18.8 mm, and 25 mm, respectively. Argon gas flows of 0.31 L/min, 7.2 L/min, and 4.2 L/min and helium gas flow rates of 31 L/min, 72 L/min, and 42 L/min were supplied through the three channels, respectively. Three turns were used for the primary RF coil with an 11 kW excitation power, 13.56 MHz excitation frequency, and a diameter of 8 mm. A temperature of 10,000 K was achieved for the pure argon simulation at the beginning of the main separation chamber, shown in Figure 5a.

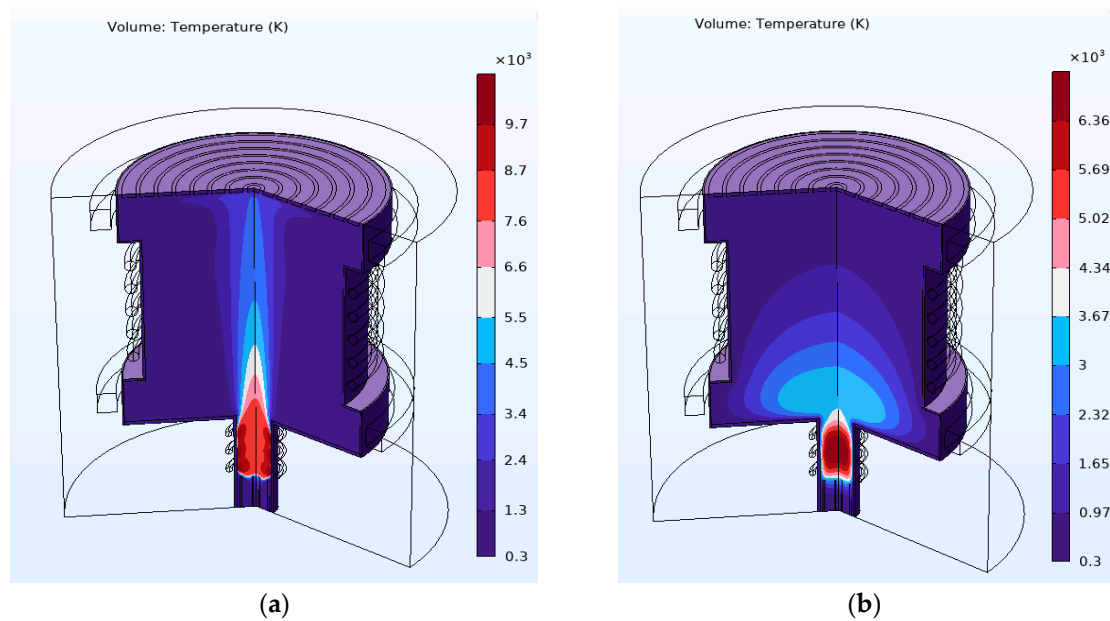


Figure 5. Primary RF ICPT simulation with 11 kW RF power, 13.56 MHz frequency, and a 0.12 m/s gas velocity; (a) argon, (b) helium.

Now, changing the plasma gas to pure helium, a temperature of 6500 K was achieved at the beginning of the main separation chamber with the same coil excitation power, shown in Figure 5b. We know at LTE that $T = T_e = T_i = T_g$, where $T = \text{plasma temperature}$, $T_e = \text{electron temperature}$, $T_i = \text{ion temperature}$, and $T_g = \text{gas temperature}$, are all considered in the thermohydraulic equilibrium. Although the T_e for helium is almost twice the argon plasma, helium has ten times higher first excitation potential under the same operating conditions, leading to a much lower electron density for helium plasma. This leads to more deviation of plasma temperature in equilibrium for helium than argon plasma [41]. The temperature for argon and helium ICP does not change much with increasing power. At the same time, increasing the inlet velocity raises the plasma axially. A temperature close to 10,000 K can partially ionize the radioactive waste and prepare for mass separation.

In the second simulation stage, primary and central RF ICP were provided with the same RF power and excitation frequency and kept the same gas velocity at the primary inlets. The central RF coil has a diameter of 15 mm and five turns. With both primary and main RF ICPT active, an average temperature inside the separation chamber reaches over 7000 K for pure argon gas ICP (Figure 6a) and over 4000 K for pure helium gas ICP (Figure 6b). It should also be mentioned that the coil's power and plasma are strongly coupled here. This means electron heating only occurs in the region of the skin depth of the plasma. According to Bahour et al., in the intense region of the plasma, the electron and ion density show similar evolution [42], which is also the case here in ED conditions assuming fully ionized plasma. With a frequency of 13.56 MHz, the plasma is more uniform in density in argon ICP than in helium ICP.

The next stage of the simulations was carried out by applying mass separation conditions using a cross-electric and magnetic field into the previous stage's plasma while keeping the primary and main RF ICPT to the same excitation power, coil frequency, and plasma gas velocity at the inlets. Two electromagnets located at the opposite end of the central RF coil were provided with a 2.5 kA current to generate a 253 G (0.0253 T) magnetic field in the axial direction of the chamber. Additionally, an electric field in the radial direction was induced into the plasma via 25 V DC voltage to the central most concentric ring electrode at the end of the chamber. A parabolic electric field profile was introduced by gradually lowering the applied voltage to the later concentric rings. A mass cutoff point,

6 amu, calculated with Equation (3) using Table 5 parameters, was applied in argon and helium plasma.

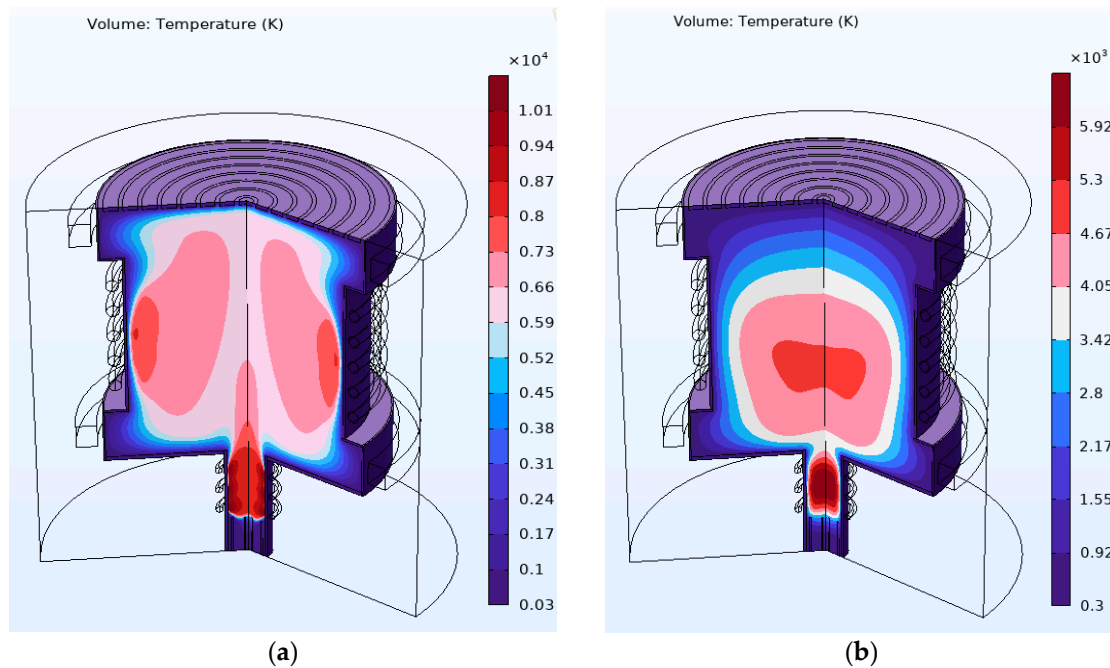


Figure 6. Plasma temperature distribution inside the separation chamber with primary and main RF ICPT is active; (a) argon (b) helium.

With the applied cross-electric and magnetic field fully coupled with the plasma physics, a lower temperature was observed, shown in Figure 7a, at the center of the chamber and higher close to the radial wall for argon ICP. On the other hand, Figure 7b shows a lower temperature close to the radial wall, and a much higher temperature is observed at the center of the chamber for helium ICP, an opposite behavior compared to the argon ICP. Under ED plasma simulation in COMSOL, the plasma is simulated in partial or complete LTE conditions where the electron temperature T_e is approximately equal to the gas T_g or ion T_i temperature. According to Bahouh et al. [42] and Lei et al. [43], in ICP plasma, in atmospheric pressure and laminar flow, the electron and heavy ion temperature follow the same particle density distribution. The hottest region has high electron and heavy ion density and vice versa in the coldest region of the plasma, confirming the LTE condition. In the ED interfaces, the plasma is assumed to be fully ionized or close to it. This means that the computed gas density is the plasma density. However, this is only true if the temperature is high enough. So, Figure 7a,b shows an apparent mass separation of noble gases under the 6 amu cutoff mass condition, where the low-mass helium ions are concentrated in the central region of the separation chamber and the high-mass argon ions are observed to be concentrated in the radial edge of the separation chamber.

In the next stage of the simulations, we focused on the mass separation effect changing the cutoff point, using Equation (3), by keeping the electric field constant and varying the magnetic field by varying the current in the electromagnetic coils listed in Table 6 below,

Table 6. List of cutoff points considered for mass separation observation.

Current (kA)	Magnetic Field (T)	Cutoff Point (amu)
2.5	0.0253	5.97~6
3	0.314	9
3.5	0.0358	12

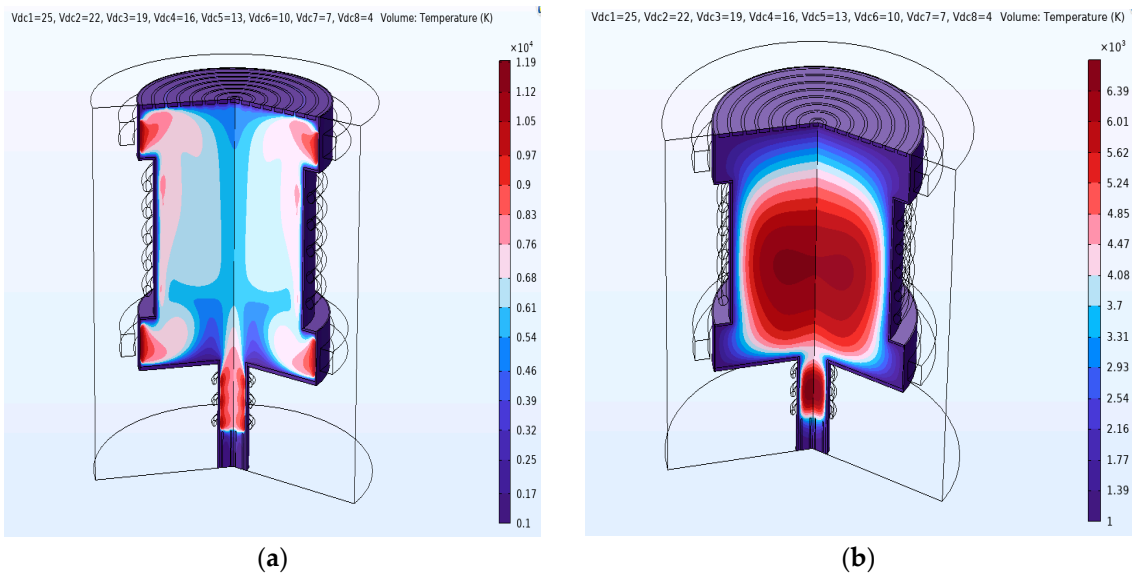


Figure 7. Plasma temperature distribution inside the separation chamber under a mass separation condition of cross electric and magnetic field for noble gas plasma; (a) argon, (b) helium, when a mass cutoff point is set to 6 amu.

In the case of argon plasma, the separation effect of raising the cutoff point is shown in Figure 8a,b, where changing the mass cutoff point from 6 amu (Figure 7a) to 9 amu (Figure 8a) and 12 amu (Figure 8b) creates a colder region in the chamber’s center as more argon ions are separated radially.

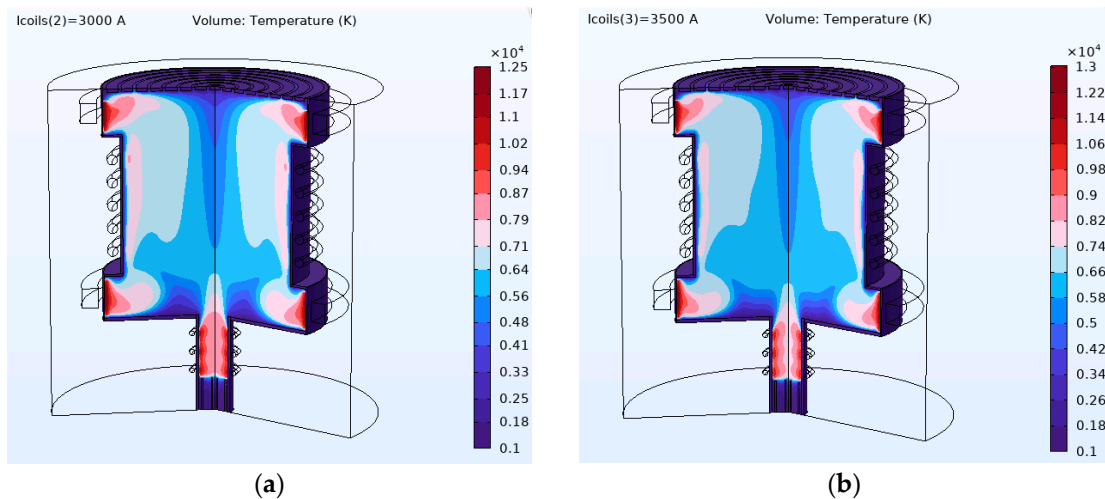


Figure 8. Effect of change in plasma temperature distribution inside the separation chamber under mass separation condition by changing the mass cutoff point; (a) 9 amu (b) 12 amu for argon plasma.

A further simulation in the case of helium plasma observes the separation effect of raising the cutoff point from 6 amu (Figure 7b) to 9 amu (Figure 9a), creating the hottest region in the center as more helium ions are concentrated in the center. Additionally, changing the mass cutoff from 9 amu to 12 amu (Figure 9b) slightly changes the temperature in the center.

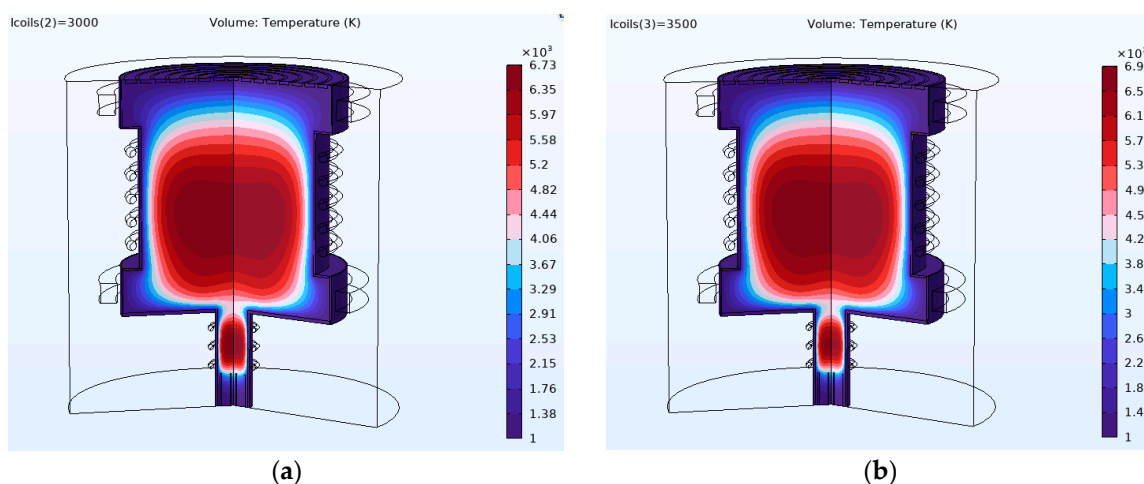


Figure 9. Effect of change in plasma temperature distribution inside the separation chamber under mass separation condition by changing the mass cutoff point; (a) 9 amu (b) 12 amu for helium plasma.

A summary of the multiphysics simulations conducted in COMSOL Multiphysics for different noble gas ICP plasma is tabulated in Table 7 below.

Table 7. Summary of multiphysics simulation on noble gas plasmas.

Simulation	RF Power	Magnetic Field (T)	Electric Field	Comments	
				Argon ICP	Helium ICP
Primary RF ICP	11 kW			T > 10,000 K	T > 6500 K
Primary RF and main RF ICP	11 kW			Average T > 6000 K inside the chamber	Average T > 4000 K inside the chamber
Mass separation condition	11 kW	0.0253 G, 0.0314 G, and 0.0358 G	Maximum 25 V to the centermost ring	Hottest plasma region close to the radial wall	Hottest plasma region at the center

5. Conclusions

Currently, there is no commercial permanent HLRW disposal site in the world. HLRW mass separation provides a unique solution for HLRW for future nuclear-based power generation worldwide. Many possible mass separation processes can be helpful for HLRW mass separation, as shown in Table 1. Rotating plasma-based mass separation could be the future of how HLRW is processed. Using the band gap ion mass filter operation principle, this paper proposes a mass separation system using atmospheric-pressure plasma torches. COLSOL Multiphysics simulation of the proposed mass separation system shows a mass separation effect for noble gas plasma under a cross-electric and magnetic field under atmospheric pressure. However, generic physics and technical issues like the charge state, neutral atom separation, molecule ionization and disassociation, ion exchange and recombination, droplets, dust and nanoparticles, ion collisions, rotation speed, plasma fluctuations, radiation and off-gas processing, and many other issues must be resolved before a practical separation device for HLRW mass separation can be achieved. Furthermore, the system needs to be high-throughput and economical before an industrial-scale system can be developed for actual HLRW processing. There is a great opportunity to develop new ideas, codes, and experiments on this front. Small-scale experiments and simulations like this research work can be designed to test specific unique ideas and applications or improve existing techniques to address some issues.

Author Contributions: Conceptualization, H.A.G.; Methodology, S.A.D. and H.A.G.; Formal analysis, S.A.D.; Investigation, H.A.G.; Data curation, S.A.D.; Writing—original draft, S.A.D.; Writing—review & editing, H.A.G.; Visualization, S.A.D.; Supervision, H.A.G.; Funding acquisition, H.A.G. All authors have read and agreed to the published version of the manuscript.

Funding: The research is supported by ProFlange (Fund #231176).

Institutional Review Board Statement: Not applicable.

Informed Consent Statement: Not applicable.

Data Availability Statement: Data available on request due to restrictions e.g., privacy or ethical.

Acknowledgments: The authors would like to thank ProFlange Inc. and Mitacs for supporting this research work.

Conflicts of Interest: The authors declare no conflict of interest.

References

- International Atomic Energy Agency. Status and Trends in Spent Fuel and Radioactive Waste Management. In *IAEA Nuclear Energy Series NW-T-1.14*; STI/PUB/1799; IAEA: Vienna, Austria, 2018.
- Jeffs, E. A Nuclear Energy Revival. In *Green Energy: Sustainable Electricity Supply with Low Environmental Impact*, 1st ed.; CRC Press: Boca Raton, FL, USA, 2009; p. 83.
- World Nuclear Association. *Storage and Disposal Options for Radioactive Waste*; World Nuclear Association: London, UK, 2020.
- Council, N.R. *Disposition of High-Level Radioactive Waste through Geological Isolation: Development, Current Status, and Technical and Policy Challenges*; The National Academies Press: Washington, DC, USA, 1999. [CrossRef]
- Nechaev, A.; Onufriev, V.; Thomas, K.T. *Long-Term Storage and Disposal of Spent Fuel*; IAEA: Vienna, Austria, 1986.
- International Atomic Energy Agency. *Long Term Storage of Spent Nuclear Fuel—Survey and Recommendations*; IAEA TECDOC-1293: Vienna, Austria, 1994.
- Wald, M.L. A Safer Nuclear Crypt. *The New York Times*, 5 July 2011. Available online: <https://www.nytimes.com/2011/07/06/business/energy-environment/06cask.html> (accessed on 4 February 2023).
- U.S.NRC. Cask Storage For Spent Fuel, Engineering News-Record. Available online: <https://www.enr.com/articles/3479-cask-storage-for-spent-fuel> (accessed on 4 February 2023).
- Fetterman, A.J.; Fisch, N.J.; Based, S.; Ion, E.; Diagnostic, L. *Plasma Mass Filters for Nuclear Waste Reprocessing*; USDOE Office of Science: Princeton, NJ, USA, 2011.
- Miguirditchian, M.; Vanel, V.; Marie, C.; Pacary, V.; Charbonnel, M.C.; Berthon, L.; Hérès, X.; Montuir, M.; Sorel, C.; Bollesteros, M.J.; et al. Poinsot, Americium Recovery from Highly Active PUREX Raffinate by Solvent Extraction: The EXAm Process. A Review of 10 Years of R&D. *Solvent Extr. Ion Exchang.* **2020**, *38*, 365–387. [CrossRef]
- Peiman, W.; Pioro, I.L.; Gabriel, K.; Hosseiny, M. Thermal aspects of conventional and alternative fuels. In *Handbook of Generation IV Nuclear Reactors*; Woodhead Publishing: Sawston, UK, 2016; pp. 583–635. [CrossRef]
- Ohkawa, T.; Miller, R.L. Band gap ion mass filter. *Phys. Plasmas* **2002**, *9*, 5116–5120. [CrossRef]
- Smith, L.P.; Parkins, W.E.; Forrester, A.T. On the Separation of Isotopes in Quantity by Electromagnetic Means. *Phys. Rev.* **1947**, *72*, 989. [CrossRef]
- Parkins, W.E. The Uranium Bomb, the Calutron, and the Space-Charge Problem. *Phys. Today* **2005**, *58*, 45–51. [CrossRef]
- Bonnevier, B. Experimental evidence of element and isotope separation in a rotating plasma. *Plasma Phys.* **1971**, *13*, 763. [CrossRef]
- Krishnan, M.; Geva, M.; Hirshfield, J.L. Plasma Centrifuge. *Phys. Rev. Lett.* **1981**, *46*, 36. [CrossRef]
- Evans, P.J.; Paoloni, F.J.; Noorman, J.T.; Whichello, J.V. Measurements of mass separation in a vacuum arc centrifuge. *J. Appl. Phys.* **1989**, *66*, 115–118. [CrossRef]
- del Bosco, E.; Dallaqua, R.S.; Ludwig, G.O.; Bittencourt, J.A. Isotopic enrichment in a plasma centrifuge. *J. Appl. Phys.* **1998**, *50*, 1716. [CrossRef]
- Zweben, S.J.; Gueroult, R.; Fisch, N.J. Plasma mass separation. *Phys. Plasmas* **2018**, *25*, 90901. [CrossRef]
- Freeman, R.; Agnew, S.; Anderegg, F.; Cluggish, B.; Gilleland, J.; Isler, R.; Litvak, A.; Miller, R.; O'Neill, R.; Ohkawa, T.; et al. *Archimedes Plasma Mass; FilterConf Proc. 694*; AIP Publishing: Moran, WY, USA, 2003; p. 403. [CrossRef]
- Ahlfeld, C.E.; Wagoner, J.D.; Sevier, D.L.; Freeman, R.L. Application, design and project implementation of a plasma mass separator for enhanced high level waste processing. In *Proceedings of the Symposium on Fusion Engineering*, Tokyo, Japan, 22–27 May 2005. [CrossRef]
- Cluggish, B.P.; Anderegg, F.A.; Freeman, R.L.; Gilleland, J.; Hilsabeck, T.J.; Isler, R.C.; Lee, W.D.; Litvak, A.A.; Miller, R.L.; Ohkawa, T.; et al. Density profile control in a large diameter, helicon plasma. *Phys. Plasmas* **2005**, *12*, 057101. [CrossRef]
- Paperny, V.L.; Krasov, V.I.; Lebedev, N.V.; Astrakchantsev, N.V.; Chernikch, A.A. Vacuum arc plasma mass separator. *Plasma Sources Sci. Technol.* **2014**, *24*, 015009. [CrossRef]
- Gueroult, R.; Evans, E.S.; Zweben, S.J.; Fisch, N.J.; Levinton, F. Initial experimental test of a helicon plasma based mass filter. *Plasma Sources Sci. Technol.* **2016**, *25*, 035024. [CrossRef]

25. Smirnov, V.P.; Samokhin, A.A.; Vorona, N.A.; Gavrikov, A.V. Study of charged particle motion in fields of different configurations for developing the concept of plasma separation of spent nuclear fuel. *Plasma Phys. Rep.* **2013**, *39*, 456–466. [CrossRef]
26. Aruquipa, W.; Velasquez, C.E.; De, G.; Barros, P.; Pereira, C.; Auxiliadora, M.; Veloso, F.; Costa, A.L. Reprocessing Techniques of Lwr Spent Fuel for Reutilization in Hybrid Systems and Iv Generation Reactors. In Proceedings of the 2017 International Nuclear Atlantic Conference—INAC 2017, Belo Horizonte, Brazil, 22–27 October 2017.
27. Choppin, G.; Rydberg, J.; Liljenzin, J.-O. *Radiochemistry and Nuclear Chemistry (Google eBook)*; Butterworth-Heinemann: Oxford, UK, 2001. Available online: https://books.google.com/books/about/Radiochemistry_and_Nuclear_Chemistry.html?id=iH-ty5d92ZQC (accessed on 9 December 2021).
28. Rodríguez-Penalonga, L.; Soria, B.Y.M. A review of the nuclear fuel cycle strategies and the spent nuclear fuel management technologies. *Energies* **2017**, *10*, 1235. [CrossRef]
29. IAEA. *Nuclear Energy Series No. NF-T-3.5: Costing of Spent Nuclear Fuel Storage*; IAEA: Vienna, Austria, 2009. Available online: <http://www.iaea.org/Publications/index.html> (accessed on 12 December 2021).
30. C. Budget Office. CBO TESTIMONY Statement of Peter R. Orszag Director. In *Costs of Reprocessing Versus Directly Disposing of Spent Nuclear Fuel: Before the Committee on Energy and Natural Resources United States Senate*; C. Budget Office: Washington, DC, USA, 2007.
31. Bunn, M.; Fetter, S.; Holdren, J.P.; van der Zwaan, B. The Economics of Reprocessing versus Direct Disposal of Spent Nuclear Fuel. *Nucl. Technol.* **2003**, *150*, 209–230. [CrossRef]
32. OECD Nuclear Energy Agency. *The Cost of High-Level Waste Disposal in Geological Repositories: An Analysis of Factors Affecting Cost Estimates*; Nuclear Energy Agency: Paris, France, 1993; p. 147. Available online: https://www.oecd-nea.org/jcms/pl_13006/cost-of-high-level-waste-disposal-in-geological-repositories-the?details=true (accessed on 12 December 2021).
33. IAEA. *TECDOC No. 1587: Spent Fuel Reprocessing Options*; IAEA: Vienna, Austria, 2009.
34. Ontario Power Generation. *New Brunswick Power, Hydro-Québec, and Atomic Energy of Canada Limited, Cost Estimate for a Deep Geologic Repository for Used Nuclear Fuel*; Ontario Power Generation: Toronto, ON, Canada, 2003.
35. Hamida, S.B.; Grandou, A.; Jankovic, M.; Eckert, C.; Huet, A.; Bocquer, J.C. A Comparative Case Study of Functional Models to Support System Architecture Design. *Procedia Comput. Sci.* **2015**, *44*, 325–335. [CrossRef]
36. Gabbar, H.A.; Darda, S.A.; Damideh, V.; Hassen, I.; Aboughaly, M.; Lisi, D. Comparative study of atmospheric pressure DC, RF, and microwave thermal plasma torches for waste to energy applications. *Sustain. Energy Technol. Assess.* **2021**, *47*, 101447. [CrossRef]
37. Sarra-Bournet, C.; Turgeon, S.; Mantovani, D.; Laroche, G. Comparison of atmospheric-pressure plasma versus low-pressure RF plasma for surface functionalization of PTFE for biomedical applications. *Plasma Process. Polym.* **2006**, *3*, 506–515. [CrossRef]
38. Thomas, S.N. *Mass spectrometry, In Contemporary Practice in Clinical Chemistry*; Academic Press: Cambridge, MA, USA, 2019; pp. 171–185. [CrossRef]
39. Ashcroft, N.W.; Mermin, N.D. *Solid State Physics*. Available online: [https://www.scirp.org/\(S\(vtj3fa45qm1ean45vvffcz55\)\)/reference/ReferencesPapers.aspx?ReferenceID=1476522](https://www.scirp.org/(S(vtj3fa45qm1ean45vvffcz55))/reference/ReferencesPapers.aspx?ReferenceID=1476522) (accessed on 14 July 2022).
40. COMSOL Multiphysics, Inductively Coupled Plasma (ICP) Torch. 2022. Available online: <https://www.comsol.com/model/inductively-coupled-plasma-icp-torch-18125> (accessed on 2 January 2020).
41. Jonkers, J.; Van De Sande, M.; Sola, A.; Gamero, A.; Van Der Mullen, J. On the differences between ionizing helium and argon plasmas at atmospheric pressure. *Plasma Sources Sci. Technol.* **2003**, *12*, 30–38. [CrossRef]
42. Bahouh, H.; Rebiai, S.; Rochette, D.; Vacher, D.; Dudeck, M. Modelling of an inductively coupled plasma torch with argon at atmospheric pressure. *Phys. Scr.* **2014**, *2014*, 014008. [CrossRef]
43. Lei, F.; Li, X.; Liu, D.; Liu, Y.; Zhang, S. Simulation study of an inductively coupled plasma discharge with different copper coil designs and gas compositions. *AIP Adv.* **2019**, *9*, 085228. [CrossRef]

Disclaimer/Publisher’s Note: The statements, opinions and data contained in all publications are solely those of the individual author(s) and contributor(s) and not of MDPI and/or the editor(s). MDPI and/or the editor(s) disclaim responsibility for any injury to people or property resulting from any ideas, methods, instructions or products referred to in the content.